7-15-2009

Asymptotic Dynamics of Attractive-Repulsive Swarms

Andrew J. Leverentz '08
Harvey Mudd College

Chad M. Topaz
Macalester College

Andrew J. Bernoff
Harvey Mudd College

SIAM J. Applied Dynamical Systems
Vol. 8, No. 3, pp. 880–908

Asymptotic Dynamics of Attractive-Repulsive Swarms*

Andrew J. Leverentz†, Chad M. Topaz‡, and Andrew J. Bernoff†

Abstract. We classify and predict the asymptotic dynamics of a class of swarming models. The model consists of a conservation equation in one dimension describing the movement of a population density field. The velocity is found by convolving the density with a kernel describing attractive-repulsive social interactions. The kernel's first moment and its limiting behavior at the origin determine whether the population asymptotically spreads, contracts, or reaches steady state. For the spreading case, the dynamics approach those of the porous medium equation. The widening, compactly supported population has edges that behave like traveling waves whose speed, density, and slope we calculate. For the contracting case, the dynamics of the cumulative density approach those of Burgers' equation. We derive an analytical upper bound for the finite blow-up time after which the solution forms one or more δ-functions.

Key words. swarm, aggregation, integrodifferential equation, attractive-repulsive, asymptotic dynamics, porous medium, Burgers' equation, blow-up

AMS subject classifications. 92, 35

DOI. 10.1137/090749037

1. Introduction.

Biological aggregations such as fish schools, bird flocks, ungulate herds, and insect swarms have drawn considerable attention from mathematical modelers in recent years. These animal groups—which for brevity we refer to simply as swarms—have implications for ecological dynamics, human food supply availability, disease transmission, and, on the longest spatiotemporal scales, evolution [19, 23]. Increasingly, they serve as prototypes for the development of algorithms in robotics, engineering, and artificial intelligence [6, 22]. Furthermore, biological swarms are a rich and versatile source of pattern-forming behavior, taking on morphologies including vortices, advancing fronts, branched dendritic structures, and more exotic patterns [12, 20].

The emergent organization of swarms can be mediated by exogenous influences such as nutrients, light, or gravity, as well as by endogenous ones, namely social interactions between individuals. Since some species swarm even in the absence of meaningful external stimuli, one concludes that social interactions play a key role. The most important social forces are thought to be attraction, repulsion, and alignment [9, 12, 13]. Attraction refers to the evolutionarily preprogrammed tendency of conspecific organisms to move towards each other, which offers benefits such as protection and mate choice, while repulsion refers to the tendency to move

*Received by the editors February 8, 2009; accepted for publication (in revised form) by J. Sneyd April 15, 2009; published electronically July 15, 2009. The first and second authors were partially supported by the NSF through grant DMS-0740484. The third author was partially supported by the NSF through grant DMS-0807347.
http://www.siam.org/journals/siads/8-3/74903.html
†Department of Mathematics, Harvey Mudd College, Claremont, CA 91711 (aleverentz@gmail.com, ajb@hmc.edu).
‡Department of Mathematics and Computer Science, Macalester College, St. Paul, MN 55105 (ctopaz@macalester.edu).

away, for instance, for collision avoidance [19]. Attraction and repulsion are driven by the relative locations of organisms. In contrast, alignment refers to the tendency of an organism to match the speed and orientation of its neighbors.

As highlighted in [12], the particular combination(s) of attraction, repulsion, and alignment that are included in a model strongly affect the classes of solutions observed. For example, [12, 13] have elucidated the importance of alignment in giving rise to diverse and exotic swarming patterns including pulses, breathers, and ripples. In contrast, models including attraction and repulsion as the only social forces have a history of several decades and an extensive literature, much of which is reviewed in [18]. These models typically give rise to groups that spread, contract, or reach equilibrium [18, 25, 26]. If organisms are self-driven in addition, milling and migrating groups may form [11, 16, 17].

In mathematical descriptions of swarms, a common modeling assumption is that social interactions take place in a pairwise manner, and that the effect of multiple organisms on a given organism can be determined via a superposition. Consider a swarm with a sufficiently large population such that the group is well described by a continuum density $\rho(\vec{x}, t)$, as in [8, 17, 25, 26] and many others. Under the aforementioned modeling assumptions, social forces involve a convolution term of the form

$$\int f_s(\vec{x} - \vec{y})\rho(\vec{y}, t)\, d\vec{y} \equiv f_s * \rho. \tag{1.1}$$

Here f_s is a kernel describing the social influence of the population at location $\vec{y}$ on that at location $\vec{x}$. Not only does the choice of social forces included in a model play a key role (as mentioned above), but the particular shape of the social kernel f_s used to model a given social force can have a crucial affect on the dynamics of the group. For instance, the particular shape of the attractive-repulsive kernel used in [8, 11] determined whether groups collapsed into a dense group, formed a well-spaced vortex-like swarm, formed a ring-like structure, or took on one of several other morphologies.

If modelers are without explicit biological measurements giving an idea of a particular organism's social kernel, they face a crucial question: in order to construct a model that gives the qualitatively correct swarming behavior, what kernel should be chosen? One might think that since the kernel is a function, it determines an infinite-dimensional parameter space, and so selecting a particular point in that space for one's model might be challenging. In practice, modelers typically choose a functional form that is presumed to be phenomenologically appropriate, for instance, a kernel f_s that is exponentially decaying in space and has the correct near-field and far-field behavior. For a few examples, see Table 1 in [18]. Even with such constraints, models may contain many parameters. For instance, there are five parameters controlling the social interactions used in [16], and at least eleven in [13].

In this paper we analyze a given class of swarming models with a general social interaction kernel, and we classify and predict the possible asymptotic dynamics. The class of models we consider is

$$\rho_t + (\rho v)_x = 0, \tag{1.2a}$$

$$v = \int_{-\infty}^{\infty} f_s(x - y)\rho(y)\, dy \equiv f_s * \rho. \tag{1.2b}$$

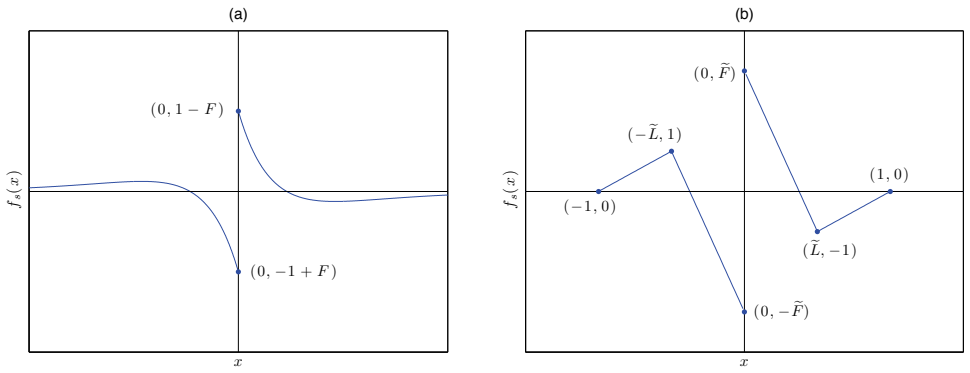

Figure 1. *Schematic depiction of f_s, the social interaction kernel in (1.2). (a) The Morse-type social force given by (1.3) for the case $F < 1$, $L > 1$. (b) The piecewise-linear social force given by (5.4) for the case $\widetilde{F} > 0$.*

This equation describes a conserved continuum density field $\rho(x,t)$ on the real line. The velocity $v(x,t)$ depends exclusively on social interactions by means of a convolution with a kernel f_s describing attraction and repulsion. In this paper, we focus solely on attractive-repulsive interactions and hence do not consider social forces with an intermediate neutral zone as in, e.g., [14]; nor do we consider alignment. This model is kinematic, as opposed to dynamic, in which case the velocity would obey a momentum equation. As reviewed in [13], social forces take place when animals communicate, either directly by auditory, visual, olfactory, or tactile senses, or indirectly, as mediated by chemical, vibrational, or other sorts of signals. A given type of communication may be unidirectional, as with visual sensing, or omnidirectional, as with auditory and olfactory sensing. Many organisms can process a combination of different input signals, which results in communication that is effectively omnidirectional [13, 21]. For this reason, in our one-dimensional model we choose f_s to describe antisymmetric social forces; that is, we assume that f_s is an odd function to ensure that distinct organisms exert equal and opposite forces on each other. Within the framework of (1.2), when $\mathrm{sgn}(x) f_s(x) < 0$ the effective social force is attractive, and when $\mathrm{sgn}(x) f_s(x) > 0$ it is repulsive. Swarming models of the form (1.2) have been studied in [3, 4, 5] for specific choices of f_s, and in a two-dimensional setting in [25].

A common choice for f_s used in, e.g., [11, 18, 24] and quite a few other studies is the Morse interaction force

$$f_s(x) = \mathrm{sgn}(x) \left[-F e^{-|x|/L} + e^{-|x|} \right]. \tag{1.3}$$

Here, the first exponentially decaying term represents attraction with strength $F > 0$ and characteristic length scale $L > 0$. The second term, of opposite sign, describes repulsion. The problem has been nondimensionalized so that the repulsive strength and length scale are unity. Figure 1(a) shows a schematic example of (1.3) for the case $F < 1$, $L > 1$. The Morse function is, in fact, a member of the more general class of kernels

$$f_s(x) = \mathrm{sgn}(x) \left[-F g(|x|/L) + g(|x|) \right], \tag{1.4}$$

where we scale the length and magnitude of g such that it has first moment equal to 2 and $g(0^+) = 1$. Here, $g(x)$ is some suitable function: it could be a Gaussian, a compactly supported function, or one of many other choices. We analyze both the Morse function (1.3) and the more general class (1.4) in this paper. However, our goal is to analyze (1.2) with as few assumptions on f_s as possible, so we also consider cases more general than (1.3) and (1.4).

We have already assumed that f_s is odd. We make three additional, relatively weak assumptions in order to facilitate our analysis. First, f_s has a finite first moment. This assumption is consistent with the idea that organisms should not interact at very long length scales because their range of sensing is limited. Second, f_s is continuous and piecewise differentiable everywhere except for a finite jump discontinuity at the origin. The biological intuition that supports this assumption is as follows: for a given organism, the effect of other organisms in the far-field should vary continuously with distance. Small changes in distance should induce small, continuous changes in the social force. However, since f_s is odd, it is discontinuous at $x = 0$ unless $f_s(x) \to 0$ as $x \to 0$. This is a degenerate case which we exclude here since we expect organisms in close proximity to have nonzero effects on each other. Note that this assumption implicitly excludes the case of so-called "hard-core" forces that blow up at $x = 0$ [18]. Third, f_s crosses 0 for at most one value of $|x|$. We concentrate on the most biologically relevant case, when organisms are repelled at short distances (avoiding collision) and attracted at longer ranges (creating a tendency to form a swarm). This means that when two organisms are within sensing range of each other, they have a unique pairwise equilibrium distance. For completeness, we will also consider other cases captured within our modeling framework, namely some cases where organisms only repel (i.e., $f_s \geq 0$ for $x > 0$) or only attract (i.e., $f_s \leq 0$ for $x > 0$), and briefly the unbiological case where there is attraction at short distances and repulsion at large distances.

To demonstrate possible asymptotic behaviors of (1.2), we conduct numerical simulations using the Morse-type social interaction (1.3) as an example. Our simulation takes place on an infinite domain and uses a particle-based numerical method we have developed, described in the appendix. Simulations reveal three asymptotic behaviors, namely spreading, steady-state, and blow-up solutions, as depicted in Figure 2. Figure 2(a) shows a spreading solution, corresponding to a population that disperses to infinity. The population density profiles are compactly supported, with a jump discontinuity at the edge. The profiles appear to be self-similar; we discuss this issue further in section 3. Figure 2(b) shows a steady-state solution, corresponding to a localized aggregation of the population. Again, the population density drops discontinuously at the edge of the support. Steady states of (1.2) are analyzed in [2]. Figures 2(c) and (d) show two cases of solutions where the density blows up, corresponding to populations with finite attraction at short distances. In the first case, the solution forms a single clump. In the second case, the solutions form multiple, mutually repelling clumps. These clumps are, in fact, δ-functions, as we discuss in section 4.

Our main results are as follows. Via long-wave and short-wave analyses, we predict how the asymptotic dynamics depend on f_s. Specifically, the long-time behavior depends on two parameters which may be directly computed from f_s: the first moment and the limiting behavior at the origin. We perform numerical simulations of (1.2) to confirm these predictions. For the spreading case, the dynamics approach those of the porous medium equation (excluding pathological behavior, which we study in section 5). The widening, compactly supported

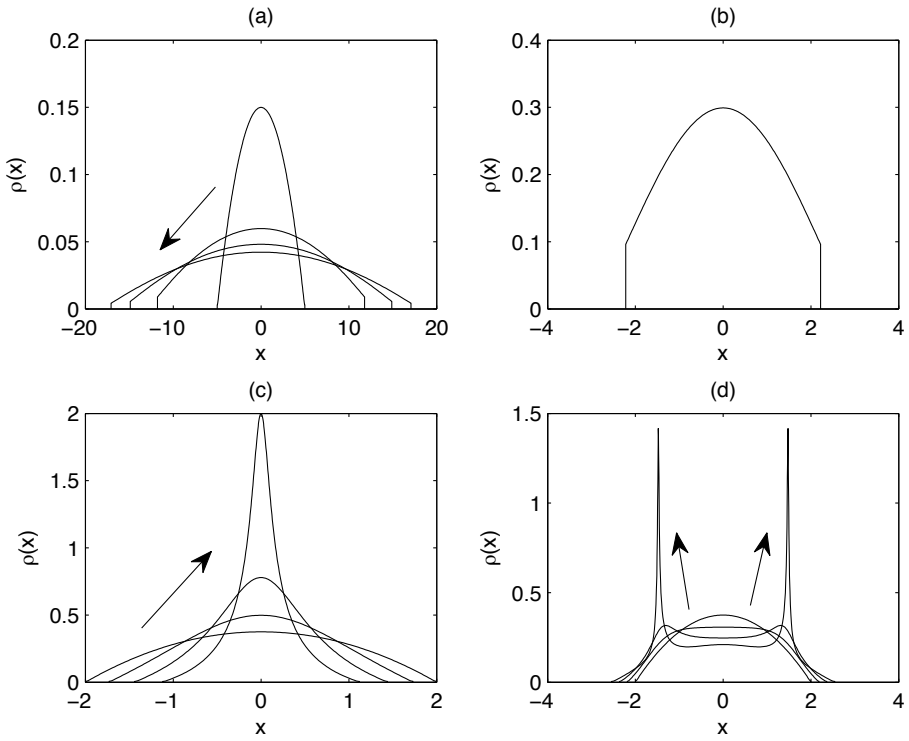

Figure 2. *Population density profiles governed by* (1.2) *with Morse-type social interactions* (1.3). *Arrows indicate the evolution of a profile over time. The asymptotic behavior of the model depends crucially on the choice of* F*, the relative strength of social attraction to social repulsion, and* L*, their relative characteristic length scales.* (a) $F = 0.2$, $L = 2$. *The compactly supported population eventually spreads to infinity.* (b) $F = 0.4$, $L = 4$. *The population reaches a compactly supported steady state.* (c) $F = 2$, $L = 2$. *The density profile blows up into a single clump.* (d) $F = 2$, $L = 0.5$. *The density profile blows up by forming mutually repulsive clumps.*

population has edges that behave like traveling waves whose speed, density, and slope we calculate. For the contracting case, the dynamics of the cumulative density approach those of Burgers' equation. We derive an analytical upper bound for the finite blow-up time after which the solution forms one or more δ-functions. The case of steady-state solutions is studied in [2].

The remainder of this paper is organized as follows. Section 2 presents basic properties of (1.2), including conservation of moments, the existence of a dissipated energy, and linear (in)stability of trivial steady states. In section 3 we study the long-wave behavior of (1.2) and show that the dynamics obey a (forward or backward) porous medium equation. In the case that long waves spread, we analyze the traveling-wave–like behavior of the edge of the swarm. In section 4 we show that the short-wave behavior obeys Burgers' equation. We examine in depth the situation when short waves contract, in which case we bound the finite blow-up time of the solution. In section 5, we combine our long- and short-wave analyses to make predictions about the asymptotic behavior of (1.2), and we confirm these with numerical simulations. We also argue that when constant-density states are linearly stable, these outcomes are exhaustive,

and we then give a pathological example where linear *instability* of these states leads to more complicated solutions. We conclude in section 6. At the end of this paper, an appendix gives an overview of a particle-based numerical method we developed to simulate our model.

2. Basic model characteristics. The model (1.2) has a number of useful properties that we now describe. First, the mass M and the center of mass $\bar{x}$, defined as

$$M(t) = \int_{-\infty}^{\infty} \rho(x,t)\,dx, \qquad \bar{x}(t) = \frac{1}{M}\int_{-\infty}^{\infty} x\rho(x,t)\,dx, \tag{2.1}$$

are both conserved. That $dM/dt = 0$ follows directly from the fact that (1.2) is formulated as a conservation law, and $d\bar{x}/dt = 0$ because of the symmetry of the social interaction force f_s. For the remainder of section 2 we show the existence of an energy that is dissipated under the dynamics, analyze the stability of trivial states, and relate their linear (in)stability to the energy.

2.1. Energy. We begin by introducing a social interaction potential $Q(x)$ associated with the social force $f_s(x)$,

$$Q(x) = -\int_{-\infty}^{x} f_s(z)\,dz. \tag{2.2}$$

From the modeling assumptions on f_s in section 1, several properties of Q immediately follow. First, $Q(x) \to 0$ as $x \to \pm\infty$ since f_s has a finite first moment. Second, $Q(x)$ is even since f_s is odd. Third, if f_s is repulsive at small distances, that is, if $f_s(0^+) > 0$, then Q has a "pointy" maximum at the origin [3]. Finally, if f_s is attractive at long distances, then $Q \to 0^-$ as $x \to \pm\infty$.

We now introduce an energy functional,

$$W[\rho] = \frac{1}{2}\int_{-\infty}^{\infty}\int_{-\infty}^{\infty} \rho(x)\rho(y)Q(x-y)\,dx\,dy. \tag{2.3}$$

For brevity, we suppress the time dependence of ρ and v in much of our analysis. The rate of energy dissipation is

$$\frac{dW[\rho]}{dt} = -\int_{-\infty}^{\infty} \rho(x)\left\{v(x)\right\}^2 dx \ < 0, \tag{2.4}$$

where $v(x)$ is defined in (1.2b). Since energy is dissipated, we conclude that stable equilibria correspond to minimizers of W.

The sign of the energy W plays an important role. For instance, we will see that spreading solutions have W tending to 0 from above. The sign of W can be assessed in a number of ways. If f_s is strictly repulsive ($Q > 0$), then $W > 0$. If $Q \geq 0$, then in fact $W > 0$ with some loose additional hypotheses. We may also derive a sufficient condition on the Fourier transform of Q for W to be positive. Define the Fourier transform

$$\widehat{g}(k) = \mathcal{F}[g(x)] = \int_{-\infty}^{\infty} g(x)e^{-ikx}\,dx. \tag{2.5}$$

Note that as $Q(x)$ is real and even, its Fourier transform is even and real. We have

$$W[\rho] = \frac{1}{2}\int_{-\infty}^{\infty}\int_{-\infty}^{\infty}\rho(x)\rho(y)Q(x-y)\,dx\,dy \tag{2.6a}$$

$$= \frac{1}{2}\int_{-\infty}^{\infty}\rho(x)\left[Q*\rho\right](x)\,dx \tag{2.6b}$$

$$= \frac{1}{4\pi}\int_{-\infty}^{\infty}|\widehat{\rho}(k)|^2\widehat{Q}(k)\,dk, \tag{2.6c}$$

where we have used the convolution theorem, Parseval's theorem, and the fact that ρ is real. We see, then, that $\widehat{Q}(k) > 0$ is a sufficient condition for $W > 0$.

2.2. Linear stability. Equation (1.2) admits steady states with constant density $\rho_0 \geq 0$. To analyze their stability, we let $\rho = \rho_0 + \widehat{\rho}e^{ikx+\sigma t}$, where k is a perturbation wave number and σ is the linear growth rate. Substituting into (1.2) and retaining only the terms linear in $\widehat{\rho}$, we obtain the dispersion relation

$$\sigma(k) = -\rho_0 k^2\widehat{Q}(k). \tag{2.7}$$

Note that $\sigma(0) = 0$ for all ρ_0 due to the conservative structure of (1.2) [10]. It follows immediately from (2.7) that the constant-density steady-state solution is linearly stable to random perturbations if and only if $\widehat{Q}(k) > 0$ for $k \neq 0$. Combined with the result of section 2.1, we see that linear stability is sufficient for the energy $W > 0$. Equivalently, if $W < 0$, then $\widehat{Q} < 0$ for some k, and constant-density steady states are linearly unstable. A similar condition is found in the dynamic model studied in [8].

3. Long-wave behavior. We consider the evolution of initial conditions that are wide and slowly varying. Specifically, assume that ρ is initially long-wave, meaning $\widehat{\rho}$ is localized near wave number $k = 0$. We show that such initial conditions evolve, at least for a short time, according to the porous medium equation. We apply the convolution theorem to (1.2b) to write the Fourier transform of the velocity as

$$\widehat{v}(k) = \mathcal{F}\{\rho * f_s\} = \widehat{\rho}(k)\widehat{f_s}(k). \tag{3.1}$$

We next write $\widehat{f_s}(k)$ as a Taylor series,

$$\widehat{v}(k) = \widehat{\rho}(k)\sum_{n=0}^{\infty}\frac{k^n}{n!}\widehat{f}_s^{(n)}(0). \tag{3.2}$$

Then, we express the nth derivative of $\widehat{f_s}$ at $k = 0$ in terms of the moments of f_s. The nth moment of f_s is

$$M_n[f_s] = \int_{-\infty}^{\infty} z^n\, f_s(z)\,dz. \tag{3.3}$$

Then,

$$\widehat{f}_s^{(n)}(0) = \left[\frac{d^n}{dk^n}\int_{-\infty}^{\infty} f_s(x)e^{-ikx}\,dx\right]_{k=0} \tag{3.4a}$$

$$= \left[\int_{-\infty}^{\infty} f_s(x)\frac{d^n}{dk^n}e^{-ikx}\,dx\right]_{k=0} \tag{3.4b}$$

$$= (-i)^n\left[\int_{-\infty}^{\infty} x^n f_s(x)e^{-ikx}\,dx\right]_{k=0} \tag{3.4c}$$

$$= (-i)^n\int_{-\infty}^{\infty} x^n f_s(x)\,dx \tag{3.4d}$$

$$= (-i)^n M_n[f_s]. \tag{3.4e}$$

Substituting (3.4e) into (3.2), we obtain

$$\widehat{v}(k) = \sum_{n=0}^{\infty}\frac{(-1)^n}{n!}(ik)^n\widehat{\rho}(k)M_n[f_s] \tag{3.5a}$$

$$= \sum_{n=0}^{\infty}\frac{(-1)^n}{n!}\mathcal{F}\left\{\frac{\partial^n\rho}{\partial x^n}\right\}M_n[f_s]. \tag{3.5b}$$

Since f_s is antisymmetric, the even moments of f_s vanish, and we have

$$\widehat{v}(k) = -\sum_{n=0}^{\infty}\frac{1}{(2n+1)!}\mathcal{F}\left\{\frac{\partial^{2n+1}\rho}{\partial x^{2n+1}}\right\}M_{2n+1}[f_s] \tag{3.6}$$

or, in physical space,

$$v(x) = -\sum_{n=0}^{\infty}\frac{M_{2n+1}[f_s]}{(2n+1)!}\frac{\partial^{2n+1}\rho}{\partial x^{2n+1}}. \tag{3.7}$$

If ρ varies on a length scale much longer than the characteristic length scale of f_s, its successive derivatives will be smaller and smaller. Assuming a nonzero first moment, we find that

$$v(x) \approx -M_1[f_s]\rho_x + \mathcal{O}(\rho_{xxx}). \tag{3.8}$$

The successively smaller error terms in (3.7) correspond to higher-order (positive or negative) diffusion. With the velocity in this form, the governing equation (1.2) becomes

$$\rho_t = \kappa(\rho^2)_{xx}, \quad \kappa = \frac{1}{2}M_1[f_s]. \tag{3.9}$$

For $\kappa > 0$, (3.9) is the well-known porous medium equation [1, 7, 28, 29], which describes the diffusion of the density. The porous medium equation is novel in that, like our evolution equation (1.2), it allows solutions with finite support. Generically, solutions to the porous medium approach a spreading, compactly supported, self-similar solution described below.

This case appears asymptotically consistent in that long-wave states in both equations will spread and therefore remain long-wave when $\kappa > 0$.

The quantity κ also has a convenient relationship to the social interaction potential Q. Specifically,

$$\widehat{Q}(0) = \int_{-\infty}^{\infty} Q(x)\,dx = \int_{-\infty}^{\infty} xq(x)\,dx = 2\kappa, \tag{3.10}$$

and so $\kappa > 0$ is a necessary condition for $\widehat{Q}(k) > 0$. Stated differently, $\widehat{Q}(k) > 0$ (and thus linear stability of constant-density states; cf. section 2.2) implies $\kappa > 0$. As we will describe in section 5, $\widehat{Q}(k) > 0$ also appears to be a sufficient condition for solutions of our swarming model to approach that of the porous medium equation at large times.

For $\kappa < 0$, (3.9) describes backwards diffusion; mathematically, this problem is ill-posed. When $\kappa < 0$, long-wave initial conditions will contract and clump until they can no longer be considered long-wave, at which point the approximations used above become invalid. Finally, we note that if $\kappa = 0$ (that is, if the first moment of f_s vanishes), the above analysis does not hold, and we must retain higher-order terms in (3.6) in order to predict asymptotic behavior.

For the remainder of this section, we focus on the spreading case $\kappa > 0$.

3.1. The Barenblatt solution for a spreading swarm. The porous medium equation (3.9) admits a class of similarity solutions due to Barenblatt,

$$\rho_*(x,t) = \frac{3^{1/3}M^{2/3}}{4[\kappa(t+t_0)]^{1/3}}\left[1 - \left(\frac{x-\bar{x}}{[9M\kappa(t+t_0)]^{1/3}}\right)^2\right]_+, \tag{3.11}$$

where we use the notation $[u]_+ = \max\{0, u\}$. Here, M and $\bar{x}$ are the conserved mass and conserved center of mass (cf. section 2), and t_0 is a parameter depending on the initial condition [28, 29]. Additionally, all finite-mass localized initial conditions for (3.9) will approach this particular class of solutions asymptotically as $t \to \infty$.

As the density profile grows wider, the long-wave approximation (3.9) will become increasingly accurate, and so we expect solutions to approach Barenblatt's solution (3.11). Figures 3 and 4 confirm this prediction. Figure 3 compares Barenblatt's solution (3.11) to numerical simulations of (1.2) using the Morse-type social force (1.3) with $F = 0.2$ and $L = 2$. For these parameters, $\kappa = 0.2 > 0$ in (3.9). The broken line represents Barenblatt's solution (3.11) for a density profile with unit mass. Under the similarity transformation

$$\widetilde{\rho}(\widetilde{x}) = \frac{1}{\gamma}\rho(\gamma x), \quad \gamma = \max_x \rho(x), \tag{3.12}$$

the spreading Barenblatt profile collapses to a single curve. The solid lines represent snapshots from the numerical simulation of (1.2). We apply to these numerical snapshots the same rescaling (3.12). We take the initial condition to be a rectangular pulse with unit mass. The direction of increasing time is indicated by the arrow in the figure. As time increases, the numerical profiles, as expected, approach the Barenblatt profile. We explore this approach further in Figure 4, which compares the root-mean-square (RMS) width of the solution. The

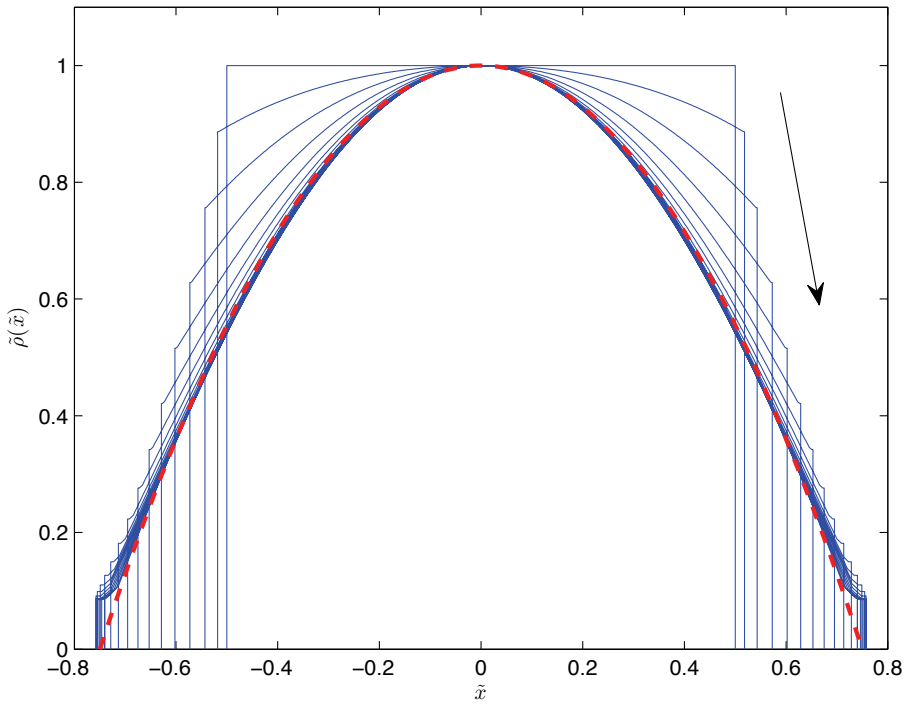

Figure 3. *Spreading solutions to (1.2) using the Morse-type social interaction (1.3) with $F = 0.2$ and $L = 2$. We choose as an initial condition a rectangular pulse with unit mass. Snapshots of the evolving profile are rescaled according to the similarity transformation (3.12). These evolving solutions are the solid curves, and the arrow indicates the time evolution. As predicted, the numerical solutions approach the idealized Barenblatt similarity solution (3.11), which has been similarly rescaled and is shown as the broken curve.*

RMS width can be computed by finding the second moment around the center of mass,

$$R \equiv \int_{-\infty}^{\infty} (x - \bar{x})^2 \rho_*(x,t)\, dy = \frac{3^{4/3}}{5} M^{5/3} \kappa^{2/3} (t + t_0)^{2/3}, \tag{3.13}$$

which yields

$$\text{RMS} = \sqrt{R/M} = \frac{3^{2/3}}{\sqrt{5}} M^{1/3} \kappa^{1/3} (t + t_0)^{1/3}. \tag{3.14}$$

From (3.14), the RMS width should grow as $t^{1/3}$. As predicted, the RMS width of the numerical solution (circles) approaches the theoretical curve (line) on the log-log plot in Figure 4.

As $t \to \infty$ the Barenblatt solution approaches zero and the energy (2.3) does as well. To see this, note that since $v(x) \approx -2\kappa\rho_x$ as $t \to \infty$ (cf. (3.8), (3.9)), the energy is

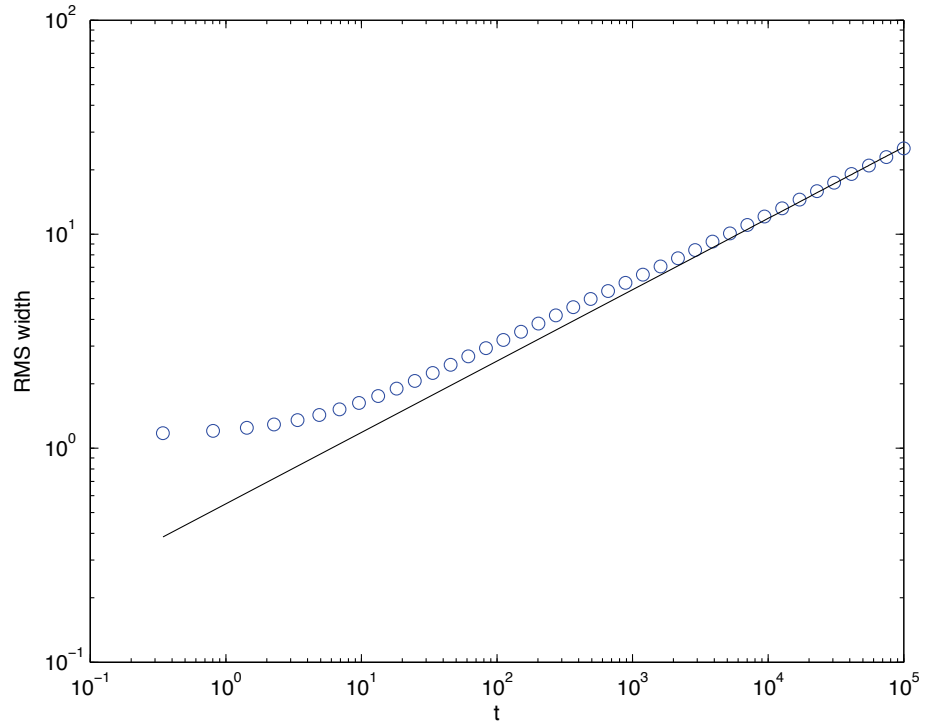

Figure 4. *RMS width of the solutions in Figure 3. The solid line represents Barenblatt's solution and has equation* $RMS = 3^{2/3}5^{-5/6}(t+t_0)^{1/3} \approx 0.544t^{1/3}$ *at large times (3.14). Circles represent the numerical solutions to (1.2), which asymptotically approach the Barenblatt spreading rate.*

$$
\begin{aligned}
W[\rho] &= \frac{1}{2}\int_{-\infty}^{\infty}\int_{-\infty}^{\infty}\rho(x)\rho(y)Q(x-y)\,dx\,dy \\
&= \frac{1}{2}\int_{-\infty}^{\infty}\int_{-\infty}^{\infty}\rho(x)\rho(y)\int_{-\infty}^{x}Q'(z-y)\,dz\,dx\,dy \\
&= -\frac{1}{2}\int_{-\infty}^{\infty}\rho(x)\int_{-\infty}^{x}\left[\int_{-\infty}^{\infty}\rho(y)f_s(z-y)\,dy\right]dz\,dx \\
&= -\frac{1}{2}\int_{-\infty}^{\infty}\rho(x)\int_{-\infty}^{x}v(z)\,dz\,dx \\
&\approx -\frac{1}{2}\int_{-\infty}^{\infty}\rho(x)\int_{-\infty}^{x}[-2\kappa\rho_z(z)]\,dz\,dx \\
&\approx \kappa\int_{-\infty}^{\infty}\rho^2(x)\,dx,
\end{aligned}
$$

which is just a constant multiple of the standard energy for the porous medium equation. Analytically, it is well known that this energy approaches zero [1]. Substituting the Barenblatt solution (3.11) yields a quantitative estimate,

$$W[\rho_*] \approx \kappa \int_{-\infty}^{\infty} \rho_*^2(x,t)\,dx = \frac{3^{1/3}M^{5/3}\kappa^{2/3}}{5(t+t_0)^{1/3}}, \tag{3.15}$$

which tends to zero as $t \to \infty$.

3.2. A traveling wave solution. Apart from the shape of the solution, we also wish to study the jump discontinuities at the edge of the spreading swarm. At the left edge of the swarm, we might expect a spreading solution to behave locally like a fixed wave profile traveling to the left (and similarly at the right edge). Therefore, we seek a traveling-wave solution to (1.2). At the left endpoint, we look for a traveling-wave solution of the form $\rho(x,t) = g(x+ct)$, where $g(z) = 0$ for all $z < 0$. Under these assumptions, (1.2) reduces to

$$0 = c\frac{\partial g}{\partial z} + \frac{\partial}{\partial z}(vg) = \frac{\partial}{\partial z}[(c+v)g]. \tag{3.16}$$

Integrating both sides of this equation,

$$(c+v)g = 0. \tag{3.17}$$

The constant of integration is zero because the left-hand side vanishes for negative z. Hence, wherever g is nonzero, $-c = v$. That is,

$$-c = \int_0^{\infty} g(\tilde{z}) f_s(z-\tilde{z})\,d\tilde{z} \quad \text{for } z \geq 0. \tag{3.18}$$

We proceed with a quantitative analysis for the example case of Morse-type social interactions (1.3). Writing out f_s explicitly and taking derivatives with respect to z on both sides (which eventually facilitates transformation of the integral equation into an ODE) yields, after some rearranging,

$$(F-1)g(z) = \frac{1}{2}\int_0^{\infty} g(\tilde{z})\left[\frac{F}{L}e^{-|z-\tilde{z}|/L} - e^{-|z-\tilde{z}|}\right] d\tilde{z}. \tag{3.19}$$

To ensure that the exponential terms are linearly independent, we assume $F \neq 0$ and $L \neq 1$. Then, to solve this integral equation, we apply the differential operators $\mathcal{L}_1 = \partial_{zz} - 1$ and $\mathcal{L}_2 = L^2\partial_{zz} - 1$ to both sides. The left-hand side becomes

$$\mathcal{L}_1\mathcal{L}_2[(F-1)g(z)] \tag{3.20a}$$

$$= (F-1)L^2 g''''(z) + (1 - F + L^2 - FL^2)g''(z) + (F-1)g(z), \tag{3.20b}$$

and the right-hand side becomes

$$\frac{1}{2}\int_0^{\infty} g(\tilde{z})\mathcal{L}_1\mathcal{L}_2\left[\frac{F}{L}e^{-|z-\tilde{z}|/L} - e^{-|z-\tilde{z}|}\right] d\tilde{z} \tag{3.21a}$$

$$= \frac{1}{2}\int_0^{\infty} g(\tilde{z}) \cdot (-2) \cdot \left[(F-L^2)\delta''(z-\tilde{z}) + (1-F)\delta(z-\tilde{z})\right] d\tilde{z} \tag{3.21b}$$

$$= (L^2 - F)g''(z) + (F-1)g(z). \tag{3.21c}$$

Hence, the integral equation (3.18) reduces to the ODE

$$g''''(z) - \alpha^2 g''(z) = 0, \tag{3.22}$$

where

$$\alpha^2 = \frac{1 - FL^2}{L^2(1-F)}. \tag{3.23}$$

Because we are in the spreading regime by assumption, $1 - FL^2 = \kappa > 0$ and $1 - F = \beta > 0$, so $\alpha^2 > 0$ and thus the coefficient on $g''(z)$ is strictly negative. Integrating the ODE twice yields

$$g''(z) - \alpha^2[g(z) - Az - B] = 0, \tag{3.24}$$

which has general solution

$$g(z) = Az + B + Ce^{-\alpha z} + De^{\alpha z}. \tag{3.25}$$

The traveling wave cannot grow exponentially as $z \to \infty$, as this would imply exponentially growing mass flux (which is proportional to the product of the speed and the derivative of the profile) as the wave translates to the left, so we choose $D = 0$. To find A, B, and C we plug (3.25) into (3.18) and simplify to obtain

$$\begin{aligned} -c = A \cdot &\left[2(FL^2 - 1) - FL^2 e^{-z/L} + e^{-z}\right] \\ + B \cdot &\left[FLe^{-z/L} - e^{-z}\right] \\ + C \cdot &\left[\frac{FL}{1-\alpha L} e^{-z/L} - \frac{1}{1-\alpha} e^{-z}\right]. \end{aligned} \tag{3.26}$$

Since $\{1, e^{-z/L}, e^{-z}\}$ are linearly independent, we can match like terms and solve the resulting three algebraic equations for A, B, and C to obtain

$$A = cA_0, \quad A_0 = \frac{1}{2(1 - FL^2)}, \tag{3.27a}$$

$$B = cB_0, \quad B_0 = \frac{1}{2(1 - FL^2)} \left(L + 1 - \frac{1}{\alpha}\right), \tag{3.27b}$$

$$C = cC_0, \quad C_0 = \frac{1}{2(1 - FL^2)} (\alpha L - 1) \left(1 - \frac{1}{\alpha}\right), \tag{3.27c}$$

which determines a traveling-wave solution for each wave speed c.

Figure 5 shows an example of the traveling left edge of the spreading swarm studied in Figures 3 and 4. We plot three snapshots of the numerically spreading solution and superpose the analytical solution given by (3.25) and (3.27). The two are in good agreement close to the edge of the support where the traveling-wave calculation above is expected to be valid.

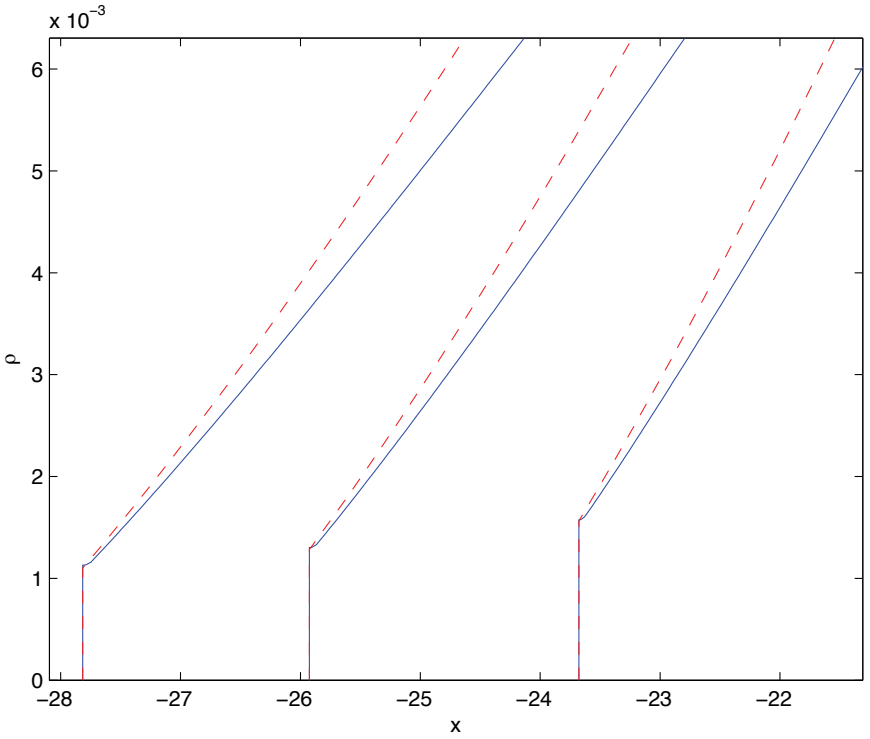

Figure 5. *Evolving left edge of the spreading solution studied in Figures 3 and 4. We superpose the analytical solution (dashed curves) given by (3.25) and (3.27) on the numerical solution (solid curves). The two are in good agreement close to the edge of the support where the traveling-wave calculation in section 3.2 is expected to be valid.*

To verify (3.25) and (3.27) further, we predict the relationship between the instantaneous speed of a traveling front, the size of the jump at the edge, and the slope of the density at the edge. In particular, the size of the jump is

$$g(0) = c(B_0 + C_0), \tag{3.28}$$

and the slope at the edge is

$$g'(0) = A - \alpha C e^{-\alpha z}\big|_{z=0} = c(A_0 - \alpha C_0). \tag{3.29}$$

A similar analysis holds at the opposite edge of the swarm. We expect these relations to hold only for large t since the solution must be sufficiently wide and slowly varying near the endpoints for it to locally approximate a traveling wave. For several values of F and L, we tested these predictions by tracking the speed, jump in density, and slope at the endpoints over time. Figure 6 shows an example that confirms the traveling-wave predictions. This example corresponds to the same spreading profile studied in Figures 3 and 4. Denote the location of the left edge of the swarm by x_e. We plot three ratios involving quantities computed at the

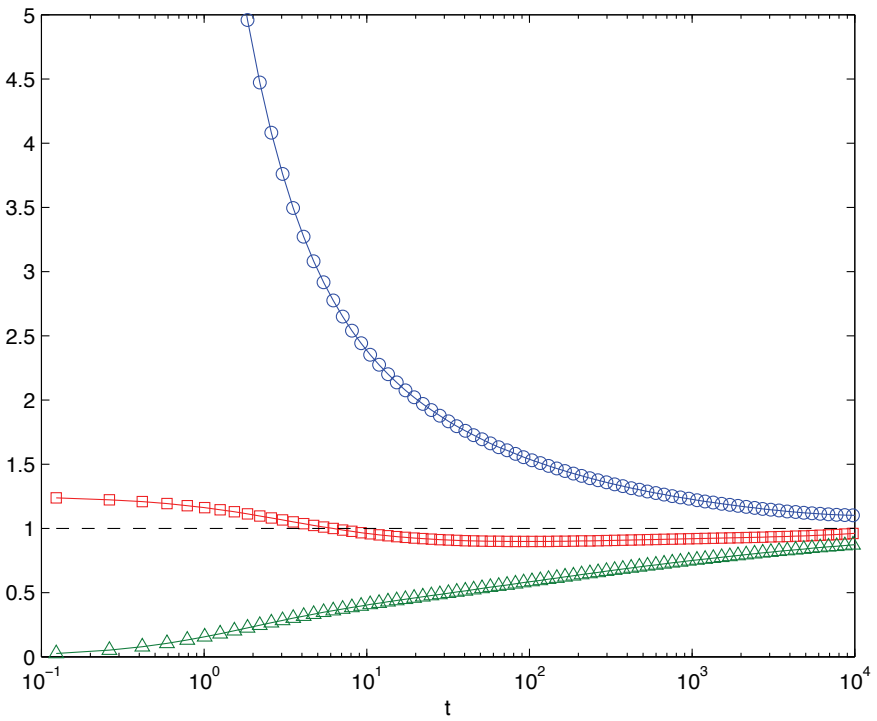

Figure 6. *Edge behavior of a spreading solution. This example corresponds to the profile studied in Figures 3 and 4. The squares, triangles, and circles indicate, respectively, the three ratios in (3.30). These quantities all approach unity (horizontal dotted line) for large t, which indicates that the asymptotic dynamics of the endpoints obey the results of the traveling-wave analysis. Specifically, as predicted by (3.28) and (3.29), the jump in density and the slope of the density profile at the edge are both proportional (via known constants) to the speed at which the edge moves.*

edge, namely

$$\frac{\rho(x_e)}{c(B_0+C_0)}, \quad \frac{\rho_x(x_e)}{c(A_0-\alpha C_0)}, \quad \frac{\rho(x_e)(A_0-\alpha C_0)}{\rho_x(x_e)(B_0+C_0)}, \tag{3.30}$$

where we take as the values of $\rho(x_e)$ and $\rho_x(x_e)$ their limits approaching from the inside of the support. Each of the three quantities in (3.30) approaches unity as $t \to \infty$, as predicted by (3.28) and (3.29).

4. Short-wave behavior. We now consider the evolution of initial conditions that are narrow and sharply varying. We show that the cumulative density behaves, at least for a short time, according to Burgers' equation [5]. We first define the cumulative mass function:

$$\psi(x,t) = \int_{-\infty}^{x} \rho(z,t)\, dz. \tag{4.1}$$

Note that since $\rho \geq 0$, $\psi(x)$ increases monotonically from a value of 0 to M. We use (1.2) to write

$$\psi_t(x,t) = \int_{-\infty}^{x} \rho_t(z,t)\,dz \tag{4.2a}$$

$$= -\int_{-\infty}^{x} (\rho(z,t)v(z,t))_z\,dz \tag{4.2b}$$

$$= -\rho(x,t)v(x,t) \tag{4.2c}$$

$$= -\psi_x(x,t)v(x,t). \tag{4.2d}$$

That is, the cumulative mass function obeys

$$\psi_t + v\psi_x = 0. \tag{4.3}$$

To proceed, recall from section 1 our assumption about the social interaction force f_s, namely that f_s is continuous and piecewise differentiable everywhere except for a jump discontinuity of size 2β at the origin. Following [5], we write

$$f_s(x) = 2\beta H(x) + g(x), \tag{4.4}$$

where $\beta \neq 0$, H is the Heaviside function, and $g(x)$ is continuous and differentiable. Substituting (4.4) into (4.3) and using the fact that $H * \rho = \psi$ yields

$$\psi_t + (2\beta\psi + g * \rho)\,\psi_x = 0. \tag{4.5}$$

For convenience, and without loss of generality, let the (conserved) center of mass of ρ be $\bar{x} = 0$. Assume that ρ is initially short-wave, so that $\widehat{\rho} \approx M$ in Fourier space. In this case, the term $(g * \rho)\psi_x \approx Mg\psi_x$. Since $\psi_x \approx \rho$ is short-wave, we may further approximate this term as $Mg(0)\psi_x$. Using the fact that $g(0) = -\beta$ from (4.4) and substituting into (4.5), we have (approximately) that

$$\psi_t + (2\beta\psi - M\beta)\,\psi_x = 0 \tag{4.6}$$

for short-wave solutions. This is Burgers' equation with an additional constant velocity term. This term may be eliminated by a simple change of variables, for instance, letting $\psi \to \psi + M/2$ to obtain

$$\psi_t + 2\beta\psi\psi_x = 0, \quad \beta = \lim_{x \downarrow 0} f_s(x). \tag{4.7}$$

We now invoke standard results for Burgers' equation [27]. Since ψ is monotonically increasing in x, ψ will contract and form a shock when $\beta < 0$ and will spread when $\beta > 0$. Moreover, because $\psi_x = \rho$, a shock in ψ is manifest as a δ-function in ρ, and so we expect that ρ will blow up when $\beta < 0$ and spread when $\beta > 0$. In fact, under mild conditions on f_s, [5] shows global existence of solutions for $\beta > 0$ and gives examples of finite-time shock formation for $\beta < 0$.

The case $\beta < 0$ is asymptotically consistent; that is, short-wave initial conditions in (1.2) will contract and therefore remain short-wave when $\beta < 0$. Equation (4.7) will become an increasingly valid approximation of (1.2). However, when $\beta > 0$, short-wave initial conditions will spread until they can no longer be considered narrow, at which point the approximations

used above will fail to hold. Finally, we note that if $\beta = 0$, we are in the degenerate case where f_s is continuous at the origin. In this case, the leading-order approximation for (1.2) would involve antiderivatives of the cumulative mass function ψ.

The quantity β has a convenient relationship to the social interaction potential Q. From (4.4) it follows that

$$-Q''(x) = f_s'(x) = 2\beta\delta(x) + r(x), \tag{4.8}$$

where $r(x) = g'(x)$ is a bounded piecewise continuous function. Taking the Fourier transform, we have

$$k^2\widehat{Q}(k) = 2\beta + \mathcal{F}[r(x)]. \tag{4.9}$$

If we let $|k| \to \infty$, the Riemann–Lebesgue lemma assures that $\mathcal{F}[r(x)]$ vanishes and so

$$\lim_{|k|\to\infty} k^2\widehat{Q}(k) = 2\beta. \tag{4.10}$$

Thus $\beta > 0$ is a necessary condition for $\widehat{Q}(k) > 0$. Stated differently, $\widehat{Q}(k) > 0$ (or equivalently, linear stability of constant-density steady states) implies $\beta > 0$, in which case blow-up is impossible.

For the remainder of this section, we focus on the case when $\beta < 0$ and solutions blow up due to short-wave contraction. Biologically, this means that at short distances, organisms are attracted to each other, leading to clumping. As discussed above, the density profile ρ blows up by forming one or more δ-functions, or equivalently by the cumulative density ψ forming shocks. The space-time plot in Figure 7 shows an example. Lines represent contours of ψ in the simulation of (1.2). The value is coded by shading, indicating the characteristics of the hyperbolic problem. As we expect, the characteristics intersect and form a shock after sufficient time, corresponding to blow-up of ρ. The blow-up profiles for a large class of f_s are studied in [5], which showed finite-time blow-up for certain initial conditions when $\beta < 0$. The authors of [3] study (1.2) in dimensions two and higher for the case when $f_s \le 0$ and $\beta < 0$ and rigorously show blow-up in finite time. Below we show that, for $\beta < 0$ and any f_s satisfying our prior assumptions, sufficiently narrow initial conditions not only blow up in a finite time but accumulate into a single δ-function. In section 5 we numerically observe blow-up for $\beta < 0$, regardless of the initial conditions chosen.

When the initial condition is a single sufficiently narrow pulse, we can approximately predict when the solution will form a δ-function. Let $a(t)$ and $b(t)$ denote the position at time t of the left and right edges, respectively. Then, for $a(t) < z < b(t)$ and $b(t) - a(t)$ sufficiently small, note that

$$f_s(a(t) - z) \ge \min_{a(t)-b(t)<r<0} f_s(r) \tag{4.11}$$

$$= \max_{0<r<b(t)-a(t)} f_s(r) \tag{4.12}$$

$$= \min_{0<r<b(t)-a(t)} |f_s(r)|. \tag{4.13}$$

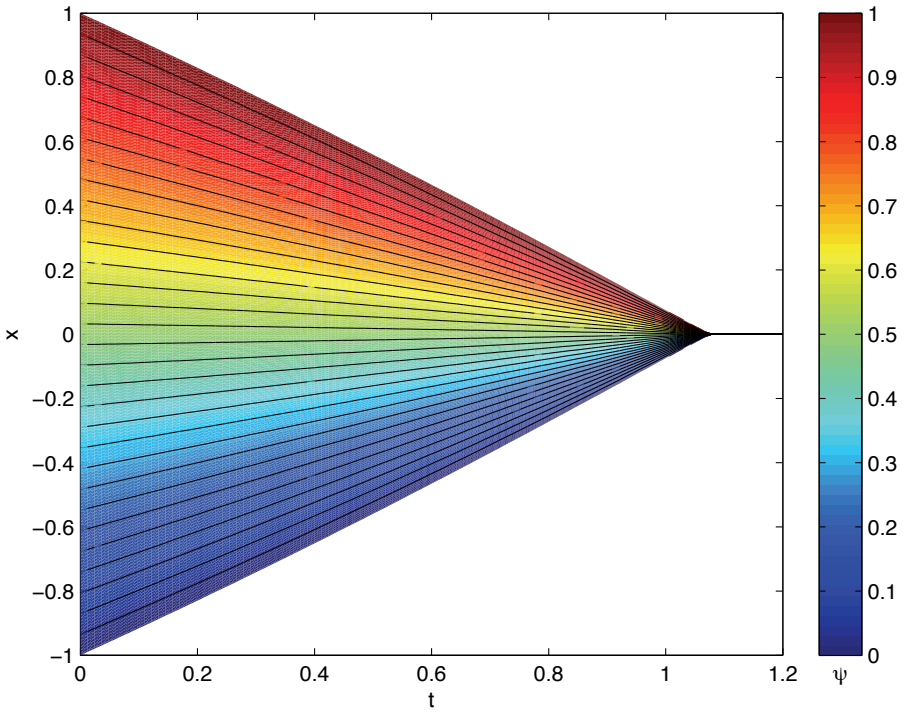

Figure 7. *Space-time plot of the cumulative mass ψ showing blow-up of the density ρ under the dynamics of (1.2). We use the Morse function (1.3) with attractive strength $F = 2$ and attractive length scale 2, for which $\beta = -1$ in (4.7). Contours of ψ appear as lines, and the value is coded by shading, indicating the characteristics of the hyperbolic problem. As we expect, the characteristics intersect and form a shock, which means that ρ blows up by forming a δ-function, as predicted.*

Here, we know $f_s(b-a) < 0$ because $b-a$ is small and positive, and because $\beta = \lim_{x \downarrow 0} f_s(x) < 0$, with f_s continuous except at the origin (cf. section 1). For convenience, define

$$q(t) = \min_{0<r<b(t)-a(t)} |f_s(r)|. \tag{4.14}$$

We find a bound for the velocity at the left endpoint:

$$a'(t) = v(a(t), t) \tag{4.15}$$

$$= \int_{a(t)}^{b(t)} \rho(z,t)\, f_s(a(t) - z)\, dz \tag{4.16}$$

$$\geq q(t) \int_{a(t)}^{b(t)} \rho(z,t)\, dz \tag{4.17}$$

$$= Mq(t) \tag{4.18}$$

$$> 0. \tag{4.19}$$

A similar argument shows that the velocity at the right endpoint satisfies

$$b'(t) \leq -Mq(t) < 0. \tag{4.20}$$

Thus, the endpoints approach each other. From (4.14) it follows that $q(t)$ must be nondecreasing, and consequently the endpoints must be accelerating towards each other or at least moving towards each other at a constant velocity.

Let t^* denote the time at which all the mass of the system enters a single δ-function. We can find an upper bound for t^* by noting

$$b'(t) \leq b'(0) \leq -Mq(0), \quad a'(t) \geq a'(0) \geq Mq(0). \tag{4.21}$$

Since the endpoints are initially separated by a distance $b(0)-a(0)$ and each is moving towards the other at a minimum speed $Mq(0)$, this gives the bound

$$t^* \leq \frac{b(0)-a(0)}{2Mq(0)}. \tag{4.22}$$

Furthermore, just before the solution forms a δ-function, by similar argumentation, the velocities of the endpoints will be $M|\beta|$ at the left endpoint and $-M|\beta|$ at the right endpoint. If $\beta = 0$ but attraction dominates at small distances, a careful analysis of $q(t)$ suggests that either finite-time or infinite-time blow-up can occur.

We have studied blow-up in numerical simulations of (1.2); results appear in Figure 8. We use the Morse-type social force (1.3) with $L = 2$. Blow-up time is shown as a function of F for two different initial conditions, namely a rectangular pulse of width 0.1 (circles) and one of width 0.2 (squares). Both sets of data closely match the analytical upper bound, indicated as solid and broken curves, respectively.

5. Global behavior of solutions. From the results in sections 3 and 4, we expect short waves to blow up when $\beta < 0$ and spread when $\beta > 0$. Similarly, we expect long waves to contract when $\kappa < 0$ and spread when $\kappa > 0$. When short waves blow up, we expect the short-wave instability to override the long-wave behavior. Finally, we will examine briefly what happens when steady states are linearly unstable, that is, when $Q(k) < 0$ for some finite value of k. Thus, we consider the following four cases:

Case (A1): When $\beta > 0$ and $\kappa > 0$, both long and short waves expand. So long as the system is in the linearly stable regime $\widehat{Q}(k) \geq 0$, solutions will spread as shown in Figure 2(a). The asymptotic dynamics of the density are governed by the porous medium equation (3.9), as discussed in section 3.

Case (A2): When $\beta > 0$ and $\kappa > 0$ but steady states are linearly unstable, i.e., $\widehat{Q}(k) < 0$ for some finite k, we expect pathological behavior with structures developing on length scales associated with the instability.

Case (B): When $\beta > 0$ and $\kappa < 0$, short waves spread while long waves contract, leading to steady-state solutions of the type shown in Figure 2(b). We analyze these solutions in depth in [2].

Case (C): When $\beta < 0$, short waves contract and solutions blow up regardless of the value of κ, leading to solutions of the types shown in Figure 2(c) and (d). The asymptotic dynamics of the cumulative density are governed by Burgers' equation (4.7), as discussed in section 4.

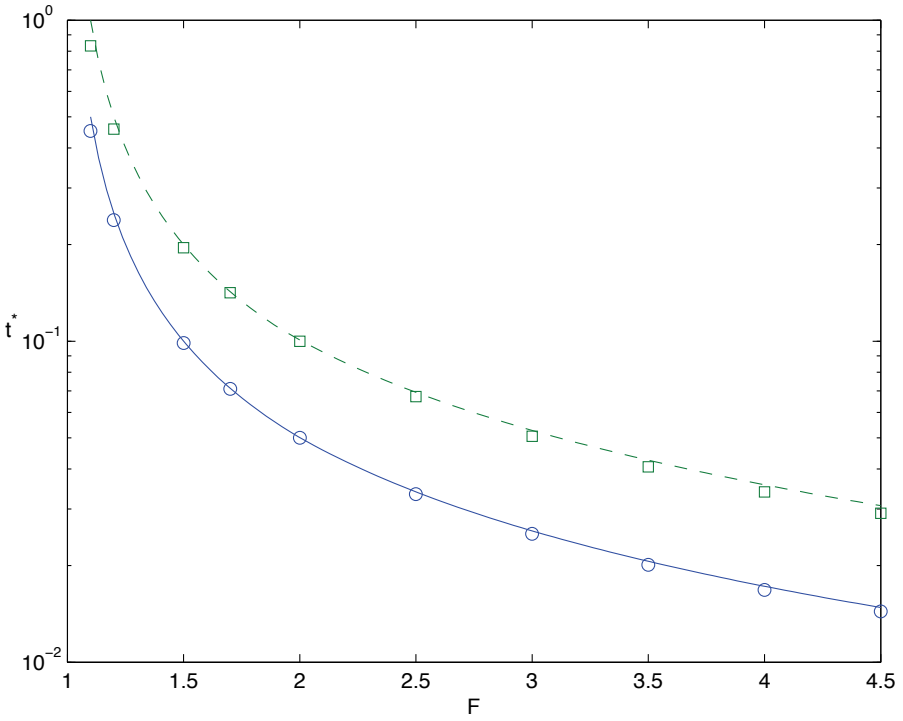

Figure 8. *Blow-up times t^* for (1.2) with Morse-type interactions (1.3). We set $L = 2$ and vary F. Data correspond to two sets of initial conditions, namely a rectangular pulse of width 0.1 (circles) and one of width 0.2 (squares). The actual blow-up times are well approximated by the analytical upper bound (4.22), indicated as the solid and broken curves.*

We first consider the generic cases (A1), (B), and (C) and then discuss the pathological case (A2) at the end of this section.

5.1. Phase diagrams for asymptotic behaviors. As an example we consider the class of social forces (1.4), for which $\kappa = 1 - FL^2$ and $\beta = 1 - F$. (Note that the regime $F > 1$, $L > 1$ corresponds to purely attractive social forces, and the regime $F < 1$, $L < 1$ corresponds to purely repulsive social forces.) We expect to see blow-up when $F > 1$, spreading when $F < 1/L^2$ and $F < 1$ (so long as $\widehat{Q} \geq 0$), and steady-state solutions when $1 > F > 1/L^2$. These predictions are indicated in Figure 9 which shows F-L parameter space. The blow-up boundary $\beta = 1 - F = 0$ is the solid line, and the spreading/steady-state boundary $\kappa = 1 - FL^2 = 0$ is the solid curve. The symbols in Figure 9 summarize the results of numerical simulations conducted for the particular case when f_s is the Morse function (1.3). The theoretical curves divide the numerical results, as expected. Our Figure 9 is similar to "phase diagrams" showing the linear stability and statistical mechanical H-stability of other swarming models with Morse-type social forces in [8, 11].

We continue this example by discussing some details of the spreading and blow-up regimes. First, recall that in our predictions above, we mentioned that, for $\beta > 0$ and $\kappa > 0$, solutions will spread unless $\widehat{Q}(k) < 0$ for some k, in which case other behavior, Case (A2), is possible.

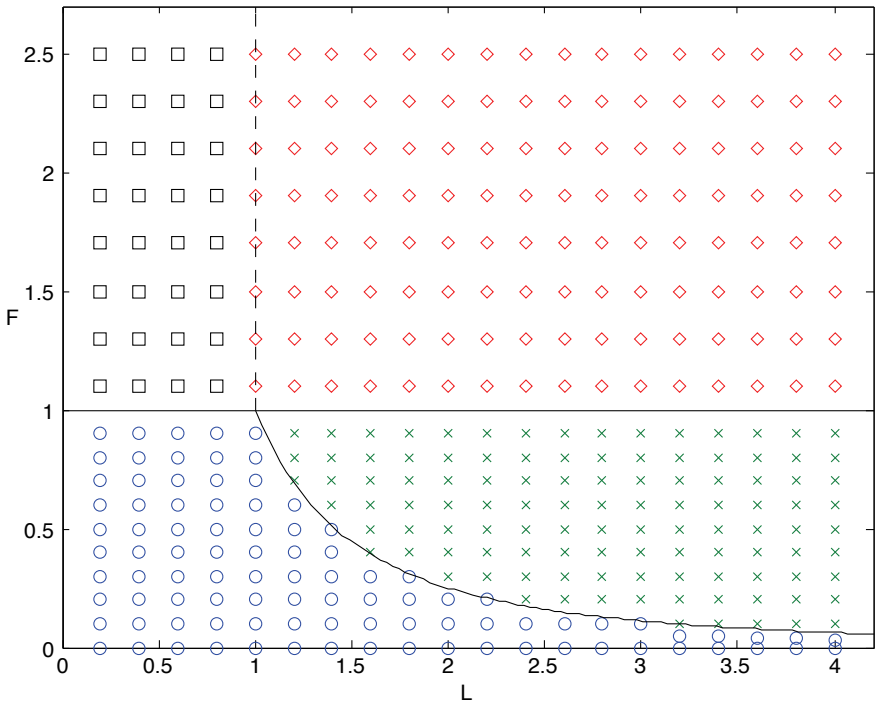

Figure 9. *Different dynamical regimes of the governing equation (1.2) in F-L parameter space for social forces of the form (1.4). F is the relative strength of attraction to repulsion, and L is the relative length scale. The solid horizontal line at $F = 1$ indicates $\beta = 0$ in (4.7) and marks the theoretical boundary above which solutions blow up. The solid curve $F = 1/L^2$ indicates $\kappa = 0$ in (3.9) and marks the theoretical boundary between spreading and steady-state solutions for $F < 1$. Results of numerical simulations using Morse-type social forces (1.3) are indicated by the symbols: spreading ($\circ$), steady-state (x), and blow-up ($\square$ and $\diamond$). The (dashed) line $L = 1$ indicates the critical case separating whether the long-range behavior is attractive or repulsive. In the blow-up regime with long-range attraction ($L > 1$), the solution forms a single δ-function ($\diamond$). With long-range repulsion ($L < 1$), multiple mutually repelling δ-functions form ($\square$).*

For (1.3), the Fourier transform of the potential is

$$\widehat{Q}(k) = \frac{2}{1+k^2} - \frac{2FL^2}{1+(kL)^2} \tag{5.1}$$

$$= \frac{2[(1-FL^2) + L^2(1-F)k^2]}{(1+k^2)(1+(kL)^2)} \tag{5.2}$$

$$= \frac{2[\kappa + L^2\beta k^2]}{(1+k^2)(1+(kL)^2)}. \tag{5.3}$$

In the regime $\kappa > 0$, $\beta > 0$ we are guaranteed $\widehat{Q}(k) \geq 0$. Thus, we are in the linearly stable regime, and pathological behavior should not be seen, as verified by the spreading numerical solutions.

Second, in the blow-up regime, we in fact observe two different types of blow-up in the

numerical simulations; the boundary between these is indicated as the broken vertical line. The particular form of the blow-up depends on the long-range character of the social force f_s. For the class of kernels (1.4), when $L > 1$, $f_s(x) \to 0^-$ as $x \to \infty$, so social forces are attractive at long distances. In this case, the entire mass of the system eventually collapses into a single δ-function. In the other case $L < 1$, $f_s(x) \to 0^+$ as $x \to \infty$, and social forces are repulsive at long distances (a behavior which does not have an immediate biological interpretation). Blow-up still occurs due to the contraction of short waves. However, the long-range repulsion means that the solution does not aggregate into one clump. Instead, multiple δ-functions form which repel each other and move apart.

To verify our analytical results further, we consider another example, in this case with a social force not of the form of (1.4):

$$f_s(x) = \operatorname{sgn}(x) \cdot \begin{cases} -\frac{\widetilde{F}+1}{\widetilde{L}}|x| + \widetilde{F}, & |x| \le \widetilde{L}, \\ \frac{1}{1-\widetilde{L}}|x| - \frac{1}{1-\widetilde{L}}, & \widetilde{L} < |x| \le 1, \\ 0, & |x| > 1, \end{cases} \tag{5.4}$$

where $\widetilde{F} \in \mathbb{R}$ and $\widetilde{L} \in (0,1)$. (Note that the regime $\widetilde{F} < 0$ corresponds to purely attractive social forces within the range of sensing.) A schematic picture is shown in Figure 1(b) for the case $\widetilde{F} > 0$. For $x > 0$, this function consists of the compactly supported, piecewise linear function passing through the points $(0, \widetilde{F})$, $(\widetilde{L}, -1)$, and $(1, 0)$. For $x < 0$ the function is the odd extension. The parameter $\widetilde{F}$ plays a role somewhat similar to F in (1.3) in that it determines whether the kernel is attractive or repulsive for short distances. The parameter $\widetilde{L}$ plays a role somewhat similar to L in that it determines a characteristic length scale. Equation (5.4) differs from (1.3) in that the kernel is compactly supported rather than decaying, is linear rather than exponential, and by construction is attractive (negative) at intermediate distances regardless of parameter choices.

For (5.4), $\kappa = (\widetilde{F}\widetilde{L}^2 - \widetilde{L} - 1)/6$ and $\beta = \widetilde{F}$. We expect to see blow-up when $\widetilde{F} \le 0$, spreading when $\widetilde{F} > \widetilde{L}^{-2} + \widetilde{L}^{-1} > 0$, and steady-state solutions when $0 < \widetilde{F} < \widetilde{L}^{-2} + \widetilde{L}^{-1}$. These predictions are indicated in Figure 10 which is similar to Figure 9 except that now we use a social force given by (5.4) rather than (1.3). As before, numerical simulations produce spreading solutions and steady states, both with jump discontinuities at the edges, as well as solutions that blow up. The theoretical predictions for these different regimes (curves) again divide the numerical results, as expected. For this example, one can show through a direct yet cumbersome calculation that $\widehat{Q}(k) > 0$, which explains why we see spreading (rather than pathological) behavior in the regime $\kappa > 0$, $\beta > 0$. Also, in this example, only single δ-function blow-up occurs because $f_s < 0$ at intermediate distances and our initial conditions have sufficiently narrow support. Since f_s is compactly supported, initial conditions that are sufficiently wide (or consist of sufficiently distant, separated groups) would blow up into multiple δ-functions that are stationary rather than mutually repelling.

5.2. Linear stability, energy, and a conjecture on spreading. We will provide a heuristic argument for the following conjecture: Suppose that $\rho(x,t)$ satisfies the swarming model (1.2) with a finite-mass initial condition and that the social force $f_s(x)$ satisfies the assumptions of section 1 with $f_s(0^+) = \beta > 0$. If constant-density states are linearly stable, i.e., the Fourier

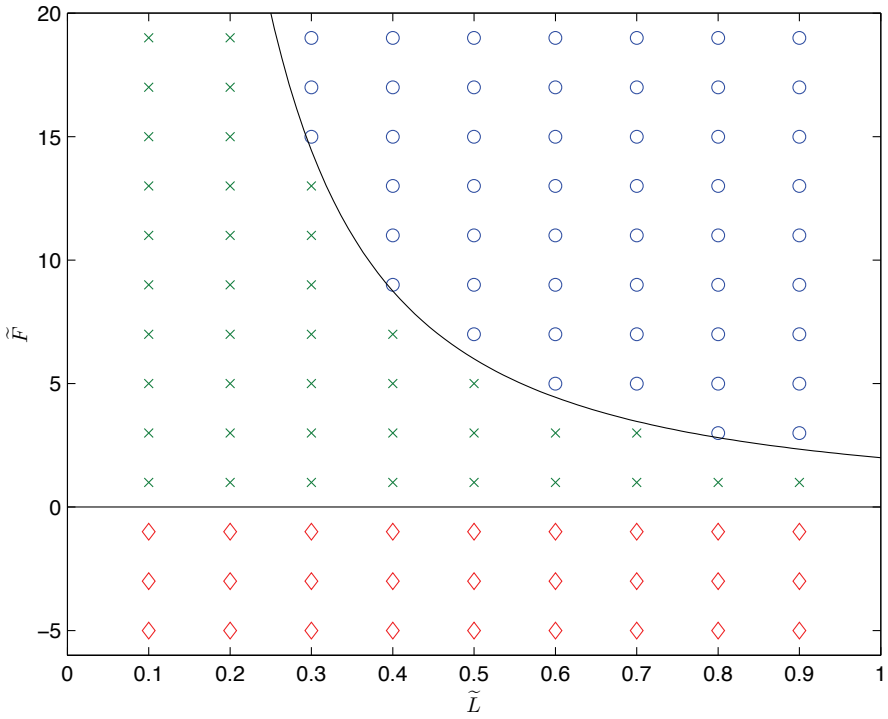

Figure 10. *Different dynamical regimes of the governing equation (1.2) in $\widetilde{F}$-$\widetilde{L}$ parameter space for the social force (5.4). The horizontal line at $\widetilde{F} = 0$ indicates $\beta = 0$ in (4.7) and marks the theoretical boundary below which solutions blow up. The solid curve $\widetilde{F} = \widetilde{L}^{-2} + \widetilde{L}^{-1}$ indicates $\kappa = 0$ in (3.9) and marks the theoretical boundary between spreading and steady-state solutions. Results of numerical simulations are indicated by the symbols: spreading (∘), steady-state (x), and single-δ-function blow-up (⋄).*

transform of the potential, $\widehat{Q}(k)$, is positive, then at large times the density converges to the Barenblatt solution of the porous medium equation.

Note that we have left the concept of convergence here consciously loose; presumably minor additional hypotheses may be needed to guarantee convergence in a particular norm.

We begin by remarking that as $\widehat{Q}(0) = 2\kappa$ under the hypotheses of this conjecture, $\kappa > 0$ and the porous medium equation derived in the limit of long waves is consistent. Similarly, as $\beta > 0$, we have global existence of solutions [5].

Since $\widehat{Q}(k) > 0$, we know that the energy $W[\rho]$ is positive as discussed in section 2.2. The dissipation of energy (2.4) guarantees that $W[p]$ is nonincreasing and $dW[\rho]/dt < 0$ unless the velocity $v(x)$ vanishes on the support of $\rho(x)$, which is equivalent to saying that $\rho(x)$ is in an equilibrium state. We will now demonstrate that there are no such equilibrium states.

Consider a steady solution $\rho(x,t) = \bar{\rho}(x)$ with support $\Omega_{\bar{\rho}}$ and finite mass. The velocity must vanish in $\Omega_{\bar{\rho}}$,

$$v(x) = \int_{\Omega_{\bar{\rho}}} f_s(x-y)\bar{\rho}(y)\,dy = 0 \qquad \text{for} \quad x \in \Omega_{\bar{\rho}}. \tag{5.5}$$

We expect $v(x)$ to be continuous, and for its derivative to vanish in $\Omega_{\bar{\rho}}$.

Consider the quantity

$$P[\rho] = \int_{\Omega_{\bar{\rho}}} \rho(x) v'(x)\, dx \tag{5.6a}$$

$$= \int_{\Omega_{\bar{\rho}}} \int_{\Omega_{\bar{\rho}}} \rho(x)\rho(y) f_s'(x-y)\, dx\, dy \tag{5.6b}$$

$$= -\int_{-\infty}^{\infty} \int_{-\infty}^{\infty} \rho(x)\rho(y) Q''(x-y)\, dx\, dy, \tag{5.6c}$$

where we have used the finite support of ρ to extend the range of integration to the entire plane. Note that $Q''(z)$ has a δ-function contribution at the origin (cf. (4.8)), but the integral is still well defined. Moreover, if this functional is evaluated on a steady solution, $P[\bar{\rho}]$ vanishes.

We can again use the convolution theorem and Parseval's theorem to show (cf. (2.6)) that

$$\begin{aligned} P[\rho] &= -\int_{-\infty}^{\infty} \int_{-\infty}^{\infty} \rho(x)\rho(y) Q''(x-y)\, dx\, dy \\ &= -\int_{-\infty}^{\infty} \rho(x) \left[Q'' * \rho\right](x)\, dx \\ &= \frac{1}{2\pi} \int_{-\infty}^{\infty} |\widehat{\rho}(k)|^2 \widehat{Q}(k)\, k^2\, dk. \end{aligned}$$

Thus, $\widehat{Q}(k) > 0$ is a sufficient condition for $P[\rho] > 0$.

Consequently, there is no steady solution $\bar{\rho}(x)$ when $\widehat{Q}(k) > 0$; otherwise $P[\bar{\rho}] = 0$, yielding a contradiction. Thus the energy dissipation rate (2.4) is negative, as $v(x)$ cannot vanish uniformly in $\Omega_{\bar{\rho}}$, and the energy is always decreasing.

In summary, the energy is decreasing and positive, and while it seems likely that the energy tends to zero at large times, we would need an estimate on the decay rate to prove this. Moreover, while it is straightforward to show that if the energy tends to zero, the width of the support of the solution must increase without bound, it is possible that the solution approaches large length scales in a manner inconsistent with our long-wave approximation. However, Occam's razor supports our conjecture; in all likelihood, the energy approaches zero via the Barenblatt solution in the manner suggested in section 3.

5.3. Pathological behavior for finite–wave number linear instability. We conclude this section with an example of the pathological behavior, Case (A2), which we have mentioned above. Consider the social force

$$f_s(x) = \operatorname{sgn}(x) \cdot \begin{cases} 1 - 2|x|^3, & |x| \le 1, \\ -e^{-(25/2)(|x|-1)}, & |x| > 1, \end{cases} \tag{5.7}$$

which is pictured in Figure 11(a). For this force, $\kappa = 0.0136$ and $\beta = 1$. As discussed, the solution should display spreading behavior if the $\widehat{Q}(k) \ge 0$ or, equivalently, if the parameters are indeed in the regime where constant-density states are linearly stable. On the other hand, if $\widehat{Q}(k) < 0$ for some k, and thus the system is in the linearly unstable regime, other behavior

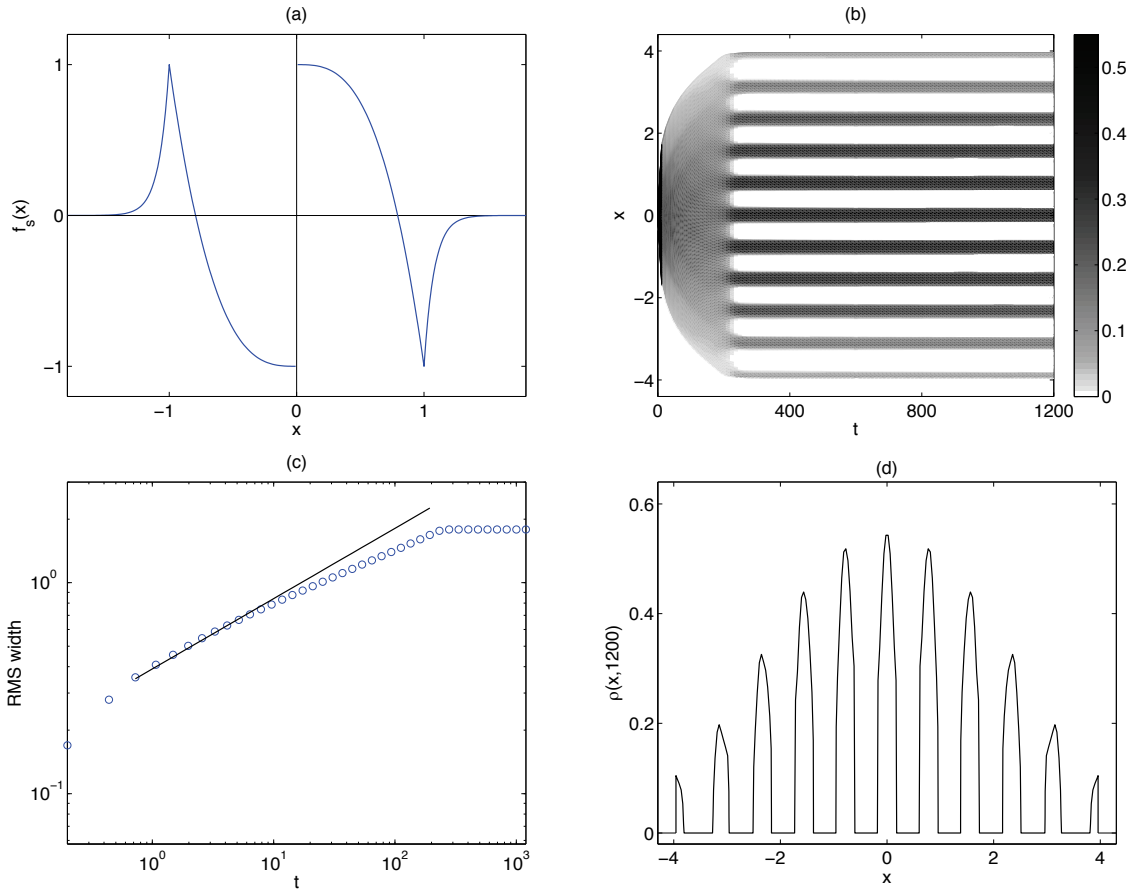

Figure 11. *Pathological behavior of* (1.2) *using the social force* (5.7). *Here,* $\kappa = 0.0136$ *and* $\beta = 1$. *Even though long and short waves both expand, the solution does not spread indefinitely because the social force is in the parameter regime where constant-density solutions are linearly unstable.* (a) *The social force* (5.7). (b) *A space-time plot of the evolving solution. Though the density profile initially expands, the spreading eventually ceases.* (c) *RMS width of the evolving solution (circles). The solid line indicates a* $t^{1/3}$ *power law that is predicted in section* 3 *for spreading solutions. For this pathological case, the* $t^{1/3}$ *Barenblatt-like behavior is seen early in the simulation, before nonlinear instability overwhelms the system.* (d) *Density profile at* $t = 1200$, *the termination of our simulation. The final state consists of* 11 *groups connected by an exponentially thin layer of density. The characteristic length scale of the pattern is approximately* 0.76, *in close agreement with the length scale predicted by linear stability analysis.*

may be seen. For (5.7), $\widehat{Q}(k)$ indeed is negative for a small region around $k_c \approx 8.2$. A space-time plot of the evolving solution of (1.2) is given in Figure 11(b) with density indicated by shading. The solution spreads for a short time, but eventually instability leads to the formation of groups. Figure 11(c) shows the RMS width of the solution (circles). The superposed line indicates a $t^{1/3}$ power law characteristic of the spreading Barenblatt solution (cf. section 3). The Barenblatt-type spreading is seen only in the early part of the simulation. Figure 11(d) shows the final state of our simulation (terminated at $t = 1200$). The equilibrium state consists of 11 individual groups connected by a very thin layer of density. We measure the

characteristic length scale of the 11-group pattern to be approximately 0.78, which matches the predication of linear analysis, namely $2\pi/k_c \approx 0.77$.

6. Conclusions. In this paper we have studied the swarming-type equation (1.2) with the goal of predicting how the asymptotic dynamics depend on the social interaction force f_s. We considered the class of social interactions that are antisymmetric (describing isotropic interactions), have finite first moments, and are continuous except at the origin. From a long-wave and a short-wave analysis, we showed that two parameters computed directly from f_s determine the asymptotic dynamics, namely the first moment 2κ and the limit approaching the origin from the right β.

As long as the system has linearly stable constant-density states (which is the case for the biologically motivated examples on which we have focused) when $\beta > 0$ and $\kappa > 0$, long and short waves both expand. As $t \to \infty$, the dynamics approach those of the porous medium equation. The shape of the profile and its spreading rate approach those of Barenblatt's well-known solution. For the case of Morse-type interactions, we calculated a quantitative relationship between the edge speed, edge density, and edge slope. Alternatively, in pathological cases where the system has linearly unstable constant-density states, the spreading solution may not be a global attractor, and pattern formation may occur.

In the case $\beta > 0$, $\kappa < 0$, long waves contract and short waves expand. In this case, the system asymptotically reaches a steady state whose shape is highly nontrivial. In [2], we analyze these solutions in detail both for the original governing equation (1.2) as well as for the case when (1.2b) contains an additional term describing exogenous forces acting on the population (for instance, the effects of gravity, light, or a nutrient field).

When $\beta < 0$, short waves contract. Regardless of the long-wave behavior, solutions blow up as $t \to \infty$. In this limit, the dynamics of the cumulative density obey Burgers' equation and form shocks; hence, the density forms one or more δ-functions.

There are several clear directions for future work. First, with the definition of the social force f_s correspondingly modified, many results from sections 3–5 could be extended to the case of higher dimensions. In particular, the predictions of the boundaries of the different dynamical regimes would be of interest. Second, though we have studied in [2] the effect of exogenous forces on steady-state solutions, we have not studied their effect on the spreading and contracting solutions that are the focus of the present paper, nor their potential effect on shifting the dynamical regime boundaries. Other extensions would include the addition of alignment forces and loosening of the restriction of omnidirectional communication, both of which would require an appropriate reformulation of the governing equations of motion. Such a study might shed light on the role parameter choices play in the models investigated in [12, 13].

We hope that our present study will guide mathematicians, biologists, and engineers who wish to construct swarming models with particular behaviors that either mimic those observed in nature or are desirable qualities for control of robotic or virtual agents. Our results suggest that, although many functional forms can be imagined for the social forces, only a few types of qualitative behavior manifest for this class of model. From another perspective, selecting a particular functional form to model social interactions is less important than choosing the parameters in that model to manifest a desired behavior. Finally, this study suggests that there are a number of characteristics inherent to kinematic models, namely, spreading parabolic

profiles, small-scale clumps, and groups with jump discontinuities at the edge, which may be used to diagnose when this class of models is appropriate.

Appendix. Numerical method. Our numerical solution of (1.2) hinges on a correspondence with a discrete model that approximates it. The paper [4] shows that a discrete model of the type we will derive converges to the continuous model under fairly weak assumptions.

Our correspondence works as follows. Consider a continuous distribution $\rho_c(x,t)$ with total mass M. For ease of notation, we suppress time dependence for the remainder of this paragraph. Define the cumulative density function

$$\psi_c(x) = \int_{x_0}^{x} \rho_c(s)\, ds, \tag{A.1}$$

where the dummy coordinate x_0 is taken to the left of the support of ρ_c. We seek a discrete approximation of N δ-function point-masses each of mass $m = M/N$. That is,

$$\rho_d(x) = \sum_{i=1}^{N} m\delta(x - x_i). \tag{A.2}$$

The associated cumulative density function ψ_d is

$$\psi_d(x) = \begin{cases} 0, & x < x_1, \\ m[1/2 + (i-1)], & x = x_i,\ i = 1, \dots, N, \\ im, & x_i < x < x_{i+1},\ i = 1, \dots, N-1, \\ M, & x > x_N, \end{cases} \tag{A.3}$$

where we have used the convention that integrating up to a δ-function yields half the mass of integrating through it. To establish a correspondence between the discrete and continuous problems, we require that $\psi_c(x_i) = \psi_d(x_i)$, which in turn determines the point-mass positions x_i. As $N \to \infty$ for fixed M, this step function ψ_d converges uniformly to ψ_c. The correspondence goes in the opposite direction as well. If we begin with an ensemble of δ-functions ρ_d, we can find the corresponding cumulative density ψ_d, interpolate to approximate ψ_c, and differentiate to find an approximate continuous density ρ_c.

With this correspondence established, we now describe our numerical method. Given an initial condition $\rho_c(x,0)$, we determine the corresponding discrete density $\rho_d(x,0)$ and the initial point-mass positions $x_i(0)$ as described above. Substituting (A.2) into the governing equation (1.2) yields a system of N ODEs:

$$\frac{dx_i}{dt} = \sum_{j \neq i} m_j f_s(x_i(t) - x_j(t)). \tag{A.4}$$

(See [18] for an introduction to discrete swarming models of this type.) We then solve the differential equations (A.4) numerically. From the new point-mass positions $x_i(t)$, we then reconstruct $\psi_d(x,t)$, $\psi_c(x,t)$, and $\rho_c(x,t)$, again using the correspondence described in the preceding paragraph.

Our numerical scheme has three sources of error. First, there is error associated with the integration of the ODEs (A.4). This error is easily controlled. We use the MATLAB routine ODE45 for the numerical solution. The second source of error is interpolation error in the construction of ρ_c from the location of the point-masses. We interpolate ψ_d to construct ψ_c and then differentiate the polynomial analytically to obtain ρ_c. The error is $\mathcal{O}(N^{-2})$. The third source of error comes from the approximation of the integral in the velocity term (1.2b). We perform this quadrature using the point-masses for collocation, with an error of $\mathcal{O}(N^{-2})$. For a full description of the numerical method and further details of the error analysis, see [15].

Acknowledgments. AJL and AJB are grateful to Harvey Mudd College for computation support. Portions of this research were conducted as part of AJL's senior thesis at Harvey Mudd College. AJB gratefully acknowledges the hospitality of Robert Kohn and the Courant Institute of Mathematical Sciences. We also wish to thank both referees for their careful and perceptive comments which greatly improved this paper.

REFERENCES

[1] D. G. Aronson, *The porous medium equation*, in Nonlinear Diffusion Problems (Montecatini Terme, 1985), Lecture Notes in Math. 1224, Springer, Berlin, 1986, pp. 1–46.
[2] A. J. Bernoff and C. M. Topaz, *Equilibrium Configurations of Interacting Particles in One Dimension*, manuscript, 2009.
[3] A. L. Bertozzi and T. Laurent, *Finite-time blow-up of solutions of an aggregation equation in* $\mathbb{R}^n$, Comm. Math. Phys., 274 (2007), pp. 717–735.
[4] M. Bodnar and J. J. L. Velazquez, *Derivation of macroscopic equations for individual cell-based models: A formal approach*, Math. Methods Appl. Sci., 28 (2005), pp. 1757–1779.
[5] M. Bodnar and J. J. L. Velazquez, *An integro-differential equation arising as a limit of individual cell-based models*, J. Differential Equations, 222 (2006), pp. 341–380.
[6] E. Bonabeu, M. Dorigo, and G. Theraulaz, *Swarm Intelligence: From Natural to Artificial Systems*, Santa Fe Institute Studies in the Sciences of Complexity, Oxford University Press, New York, 1999.
[7] J. A. Carrillo and G. Toscani, *Asymptotic* L^1*-decay of solutions of the porous medium equation to self-similarity*, Indiana Univ. Math. J., 49 (2000), pp. 113–142.
[8] Y. L. Chuang, M. R. D'Orsogna, D. Marthaler, A. L. Bertozzi, and L. S. Chayes, *State transitions and the continuum limit for a* $2d$ *interacting, self-propelled particle system*, Phys. D, 232 (2007), pp. 33–47.
[9] I. D. Couzin, J. Krause, R. James, G. D. Ruxton, and N. R. Franks, *Collective memory and spatial sorting in animal groups*, J. Theoret. Biol., 218 (2002), pp. 1–11.
[10] M. C. Cross and P. C. Hohenberg, *Pattern formation outside of equilibrium*, Rev. Mod. Phys., 65 (1993), pp. 851–1112.
[11] M. R. D'Orsogna, Y. L. Chuang, A. L. Bertozzi, and L. Chayes, *Self-propelled particles with soft-core interactions: Patterns, stability, and collapse*, Phys. Rev. Lett., 96 (2006), paper 104302.
[12] R. Eftimie, G. de Vries, and M. A. Lewis, *Complex spatial group patterns result from different animal communication mechanisms*, Proc. Natl. Acad. Sci. USA, 104 (2007), pp. 6974–6979.
[13] R. Eftimie, G. de Vries, M. A. Lewis, and F. Lutscher, *Modeling group formation and activity patterns in self-organizing collectives of individuals*, Bull. Math. Biol., 69 (2007), pp. 1537–1565.
[14] S. Gueron, S. A. Levin, and D. I. Rubenstein, *The dynamics of herds: From individuals to aggregations*, J. Theoret. Biol., 182 (1996), pp. 85–98.
[15] A. J. Leverentz, *An Integrodifferential Equation Modeling* 1*-D Swarming Behavior*, Senior thesis, Department of Mathematics, Harvey Mudd College, Claremont, CA, 2008.
[16] H. Levine, W. J. Rappel, and I. Cohen, *Self-organization in systems of self-propelled particles*, Phys. Rev. E, 63 (2001), paper 017101.

[17] A. Mogilner and L. Edelstein-Keshet, *A non-local model for a swarm*, J. Math. Biol., 38 (1999), pp. 534–570.
[18] A. Mogilner, L. Edelstein-Keshet, L. Bent, and A. Spiros, *Mutual interactions, potentials, and individual distance in a social aggregation*, J. Math. Biol., 47 (2003), pp. 353–389.
[19] A. Okubo, D. Grünbaum, and L. Edelstein-Keshet, *The dynamics of animal grouping*, in Diffusion and Ecological Problems, Interdiscip. Appl. Math. 14, 2nd ed., A. Okubo and S. A. Levin, eds., Springer, New York, 2001, Ch. 7, pp. 197–237.
[20] J. K. Parrish and L. Edelstein-Keshet, *Complexity, pattern, and evolutionary trade-offs in animal aggregation*, Science, 284 (1999), pp. 99–101.
[21] S. R. Partan and P. Marler, *Issues in the classification of multimodal communication signals*, Amer. Naturalist, 166 (2005), pp. 231–245.
[22] K. M. Passino, *Biomimicry for Optimization, Control, and Automation*, Springer, London, 2005.
[23] D. Tilman and P. Kareiva, eds., *Spatial Ecology: The Role of Space in Population Dynamics and Interspecific Interactions*, Princeton University Press, Princeton, NJ, 1998.
[24] C. M. Topaz, A. J. Bernoff, S. Logan, and W. Toolson, *A model for rolling swarms of locusts*, Eur. Phys. J. Special Topics, 157 (2008), pp. 93–109.
[25] C. M. Topaz and A. L. Bertozzi, *Swarming patterns in a two-dimensional kinematic model for biological groups*, SIAM J. Appl. Math., 65 (2004), pp. 152–174.
[26] C. M. Topaz, A. L. Bertozzi, and M. A. Lewis, *A nonlocal continuum model for biological aggregation*, Bull. Math. Biol., 68 (2006), pp. 1601–1623.
[27] G. B. Whitham, *Linear and Nonlinear Waves*, Wiley, New York, 1974.
[28] T. P. Witelski and A. J. Bernoff, *Self-similar asymptotics for linear and nonlinear diffusion equations*, Stud. Appl. Math., 100 (1998), pp. 153–193.
[29] Y. B. Zeldovich and G. I. Barenblatt, *Asymptotic properties of self-preserving solutions of equations of unsteady motion of gas through porous media*, Dokl. Akad. Nauk SSSR, 118 (1958), pp. 671–674.